Journal of Solid State Chemistry 181 (2008) 2473–2479

Contents lists available at ScienceDirect

Journal of Solid State Chemistry

journal homepage: www.elsevier.com/locate/jssc

Hyperfine interactions and lattice dynamics of $Sn_{21}O_6Cl_{16}(OH)_{14}$

M.T. Sougrati, S. Jouen, B. Hannoyer *, B. Lefez

Groupe de Physique des Matériaux, Université de Rouen, CNRS-UMR 6634, Avenue de l'Université-BP 12, 76801 Saint-Etienne du Rouvray, France

ARTICLE INFO

Article history:
Received 14 February 2008
Received in revised form
31 May 2008
Accepted 5 June 2008
Available online 14 June 2008

Keywords:
Abhurite
Tin
Tin(II) oxy-hydroxychloride
Mössbauer spectroscopy
Low temperature
Recoil-free fraction

ABSTRACT

In this study, the tin(II) oxy-hydroxychloride $Sn_{21}O_6Cl_{16}(OH)_{14}$ has been synthesised and investigated. This compound is the synthetic equivalent of mineral abhurite, which was discovered in 1985 as a tin corrosion product formed on the surface of tin ingots after long immersion in seawater. The Mössbauer parameters of $Sn_{21}O_6Cl_{16}(OH)_{14}$ determined at various temperatures are reported and discussed for the first time. At room temperature, the isomer shift and the quadrupole splitting are, respectively, $\delta = 3.22\,mm\,s^{-1}$ and $\Delta = 1.71\,mm\,s^{-1}$, relative to the centroid of the spectrum of $BaSnO_3$. The Mössbauer recoil-free fraction has been also evaluated over a wide range of temperature. At 300 K, the recoil-free fraction of $Sn_{21}O_6Cl_{16}(OH)_{14}$ is $f_{300} = 0.09 \pm 0.02$.

1. Introduction

In 1985, a new tin oxy-hydroxychloride mineral was discovered on the surface of tin ingots submerged during approximately 100 years in the Red Sea after a shipwreck [1]. It was named abhurite since its discovery locality is Sharm Abhur, located near Jeddah, Saudi Arabia. Recently abhurite has been also detected mixed with romarchite SnO and hydroromarchite $Sn_3O_2(OH)_2$, on the surface of corroded pewter artifacts remaining from the Queen Anne's Revenge wreck that sank near Beaufort, North Carolina in 1718 [2]. Abhurite stoichiometry was firstly suggested as $Sn_3OCl_2(OH)_2$ in 1985 by Matzko et al. [1]. Subsequently, it has been demonstrated that the synthetic rhombohedral tin chloride hydroxide oxide $Sn_{21}O_6Cl_{16}(OH)_{14}$ and abhurite are identical. $Sn_{21}O_6Cl_{16}(OH)_{14}$ single-crystal X-ray structure was then perfectly determined [3,4]. Numerous preparations of tin(II) hydroxychloride have been realised in the last century and various stoichiometries have been proposed. According to Edwards et al. [4], all various preparations of basic tin(II) chloride result in the formation of the same compound, $Sn_{21}O_6Cl_{16}(OH)_{14}$ and discrepancies in the various formulations claimed in the literature might be the result of the presence of tin(II) oxychlorides and adsorbed water mixed with $Sn_{21}O_6Cl_{16}(OH)_{14}$.

In corrosion science, the knowledge of the corrosion layers composition remains essential. Crystallographic data available in the literature are sufficient to perform the identification of $Sn_{21}O_6Cl_{16}(OH)_{14}$ with X-ray diffraction, and the spectroscopic parameters necessary to identify the compound by means of Fourier transform infra-red reflection-absorption spectroscopy analysis have been recently published [5]. Among the techniques of characterisation, Mössbauer spectroscopy has been demonstrated as being very effective and complementary for tin compounds study [6–9]. Mössbauer spectroscopy is a unique tool to perform structural and dynamical investigations of solids at an atomic scale. Unfortunately, most of the Mössbauer experiments concern the iron-57 nuclide resonance when only few laboratories work on the tin-119 nucleus Mössbauer effect despite the great interest demonstrated for many fields. Consequently, only scarce literature data are available on tin corrosion products and they are often incomplete and sometimes prone to controversy. The recoil-free fraction, also called *f*-factor, is a dynamic parameter of the lattice defined as the probability for recoilless emission or absorption of a γ-ray by a resonant atomic nucleus in a solid. Accurate determination of this parameter is necessary to perform quantitative analysis since it permits, in a mixture, to convert the relative Mössbauer sub-spectrum fraction of a compound to its relative atomic ratio. Contrary to iron phases, tin compounds suffer from low and disperse *f*-factor values at room temperature. Consequently, for many tin absorbers with low recoil-free fraction, the Mössbauer effect cannot be observed satisfactory at 300 K and low temperature analysis is necessary. Thus the knowledge of the Mössbauer parameters at various temperatures is required.

Mössbauer isomer shift and quadrupole splitting parameters have been already published by Von Schnering et al. [3] for the synthetic $Sn_{21}O_6Cl_{16}(OH)_{14}$ compound at room temperature. The

* Corresponding author. Fax: +33 2 32 95 50 70.
E-mail address: beatrice.hannoyer@univ-rouen.fr (B. Hannoyer).

0022-4596/$ - see front matter © 2008 Elsevier Inc. All rights reserved.
doi:10.1016/j.jssc.2008.06.020

reported parameters, $\delta = 2.81\,\mathrm{mm\,s^{-1}}$ (relative to $BaSnO_3$) and $\Delta = 1.86\,\mathrm{mm\,s^{-1}}$ are quite different from those determined in this study. This discrepancy will be discussed later.

The purpose of this work is to determine and to discuss the isomer shift and quadruple splitting of a synthesised $Sn_{21}O_6Cl_{16}(OH)_{14}$ over a broader range of temperatures ($25\,\mathrm{K} \leqslant T \leqslant 300\,\mathrm{K}$). Mössbauer lattice temperature and recoil-free fractions, necessary for quantitative analysis, will also be extracted using the technique of temperature dependence of the resonance peak.

2. Experimental

2.1. Sample preparation

Synthetic abhurite $Sn_{21}O_6Cl_{16}(OH)_{14}$ has been grown electrochemically on a tin plate surface using the protocol described in a previous paper [5]. The powder sample used for Mössbauer spectroscopy was removed mechanically from the tin corroded surface.

The powder was observed by means of scanning electron microscopy as shown in Fig. 1. It appears as thin plates assembled in spherical geometry of few micrometres of average diameter.

2.2. Investigation methods

XRD analysis was performed with a Bruker D8 equipment using the Co-$K\alpha$ radiation ($\lambda = 1.78897$ nm) and FT-IRRAS spectra with a Nicolet 710 instrument accumulating 128 interferograms in the energy range 4000–250 $\mathrm{cm^{-1}}$ at a resolution of 4 $\mathrm{cm^{-1}}$, in transmission and specular reflection modes [5]. Raman spectroscopy was performed with a Renishaw inVia Reflex System (Wotton-Under-Edge, UK), equipped with a HeNe laser (wavelength 632.8 nm). All Raman spectra were recorded with a 100 × objective lens, between 100 and 1200 $\mathrm{cm^{-1}}$ for two accumulations with the Renishaw SynchroScan system.

Transmission Mössbauer spectroscopy was conducted with a conventional constant acceleration spectrometer, using a $Ba^{119}SnO_3$ source. In this mode, the full depth of the sample is analysed and the spectrum is plotted with the number of transmitted γ-ray, collected by a proportional counter with a multichannel analyser, versus the velocity of the radioactive source. All the spectra were fitted as a sum of Lorentzian line shapes by a least-squares programme. The energy shift data are quoted relative to the centroid of $BaSnO_3$ spectrum at room temperature. The spectra were recorded over the 25–300K temperature range with a closed-cycle helium refrigerator (CCS-850, Janis Research Company Inc.). A sample chamber surrounded by a vacuum wall is cooled with a refrigerator system at 10 K. The analysed powder is suspended within a copper holder between aluminised mylar windows and is cooled indirectly using static helium exchange gas inside the sample chamber. The copper holder includes a temperature sensor and a heater, both managed by an auto-tuning temperature controller.

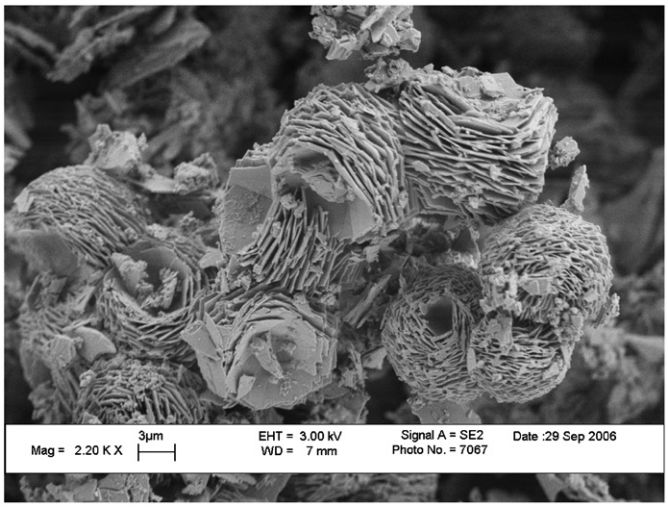

Fig. 1. Scanning electron micrograph of synthetic $Sn_{21}O_6Cl_{16}(OH)_{14}$ powder.

3. Results and discussions

X-ray pattern of the synthesised powder is shown in Fig. 2. The diffraction peaks obtained are all perfectly consistent with those of the rhombohedral space group $R32$ of abhurite (JCPDS cards 39-0314 and 72-0252). No other crystalline phase was detected. Mössbauer analysis discussed in the following section demonstrates clearly the presence of a unique tin compound. The unit-cell parameters have been determined from the XRD patterns using a 'Chekcell' routine: $a = b = 10.024 \pm 0.001$ Å and $c = 44.072 \pm 0.003$ Å in good accordance with literature data.

To complete the physico-chemical characterisation of the compound, a vibrational study was carried out. A Fourier transform infra-red spectroscopic study of this synthesised abhurite was already published by the authors [5]. To perform *in situ* analysis in corrosion studies, reflection-absorption mode is used. But it is well known that bands in reflection-absorption spectra may be shifted compared to the transmission spectrum because of the dispersion of the refractive index n. Consequently, the optical constant n and k were calculated, and so available to perform the calculation of reflection-absorption spectra at various angles and for various thicknesses of $Sn_{21}O_6Cl_{16}(OH)_{14}$. An experimental infra-red transmission spectrum is reported for illustration in Fig. 3a. The spectrum is characterised by strong absorption bands, between 3600 and 3200 $\mathrm{cm^{-1}}$, attributed to OH stretching modes. The band at 1621 $\mathrm{cm^{-1}}$ is due to bending vibrations of water. The two absorption bands at 966 and 923 $\mathrm{cm^{-1}}$ can be assigned to hydroxyl OH deformations, Sn–O–H bending modes, while the band at 634 $\mathrm{cm^{-1}}$ may be attributed to Sn–O stretching modes. The four bands at 473, 425, 363 and 328 $\mathrm{cm^{-1}}$ are in the absorption domain of fundamental vibrations of metallic ions of crystal lattice and can therefore be assigned to the Sn–O and Sn–Cl stretching modes.

The experimental Raman spectrum of our $Sn_{21}O_6Cl_{16}(OH)_{14}$ sample, is shown in Fig. 3b in the 100–600 $\mathrm{cm^{-1}}$ region. This spectrum is in good agreement with the Raman spectrum of mineral abhurite collected in the RRUFF database of Raman spectroscopy (Fig. 3b) [10]. However, intensity modification of Raman bands is observed because of different wavelength laser

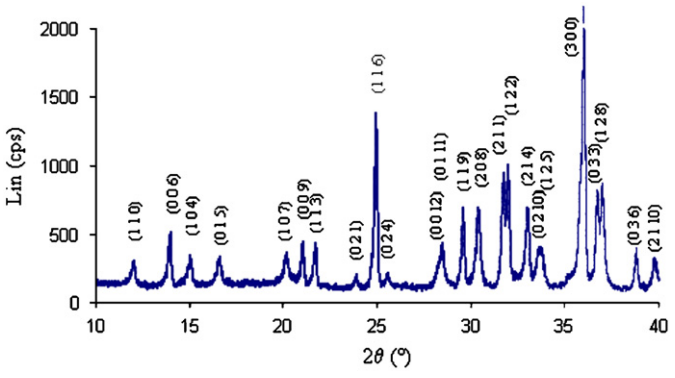

Fig. 2. X-ray pattern of the synthesised $Sn_{21}O_6Cl_{16}(OH)_{14}$.

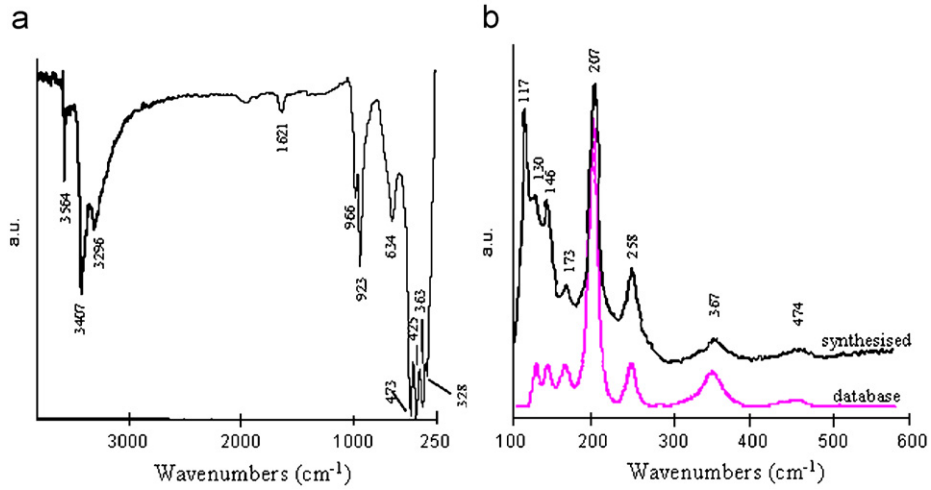

Fig. 3. (a) Transmission infra-red spectrum of the synthesised $Sn_{21}O_6Cl_{16}(OH)_{14}$. (b) Raman spectrum of the synthesised $Sn_{21}O_6Cl_{16}(OH)_{14}$ compared to the spectrum of abhurite from the RRUFF database of Raman spectroscopy [10].

excitation and sensitivity of CCD detectors used. There is no report, to our knowledge, on the characteristic spectral frequencies of the abhurite pattern. Vibrational modes in the spectral range 100–400 cm^{-1} are usually associated with lattice modes vibration. This spectral region, with two prominent bands observed at 117 and 207 cm^{-1}, may be assigned to lattice modes vibration Sn–O and Sn–Cl. A detailed study is under investigation.

4. Mossbauer study of $Sn_{21}O_6Cl_{16}(OH)_{14}$

4.1. Temperature dependence of Mössbauer parameters

The relevant hyperfine parameters of $Sn_{21}O_6Cl_{16}(OH)_{14}$, obtained from Mössbauer spectrum recorded in transmission geometry at room temperature, are summarised in Table 1. Mössbauer spectra obtained at various temperatures in the range 25–300 K are shown in Fig. 4. They present the same shape with a unique doublet, without any other contribution except the small one around 0 mm s^{-1} due to the air oxidation of the powder, detectable at 300 K but enhanced by the *f*-factor effect and under the limit detection at low temperature. This confirms the purity of the synthesised compound. The line widths Γ of the two components of the doublet are very close and increase, from 0.94 to 1.16 mm s^{-1}, with decreasing temperature. These values are of the same order of magnitude as line width of many tin(II) species.

At 300 K, the spectrum exhibits an isomer shift δ of 3.22 mm s^{-1} and a quadrupole splitting Δ of 1.71 mm s^{-1}, in agreement with a divalent tin compound. These values are not in accordance with the unique set of Mössbauer parameters of $Sn_{21}O_6Cl_{16}(OH)_{14}$ available in the literature, published by Von Schnering et al. [3], $\delta = 2.81$ mm s^{-1} and $\Delta = 1.86$ mm s^{-1}. In fact, although the parameters published are those of only one doublet, Von Schnering mentions that the spectrum consists of four doublets, indicating the existence of four crystallographic different Sn(II) environments. This information is somewhat contradictory and, unfortunately, without layout of the spectrum it is not possible to appreciate the deconvolution of the doublet.

According to the same authors, the crystal structure of $Sn_{21}O_6Cl_{16}(OH)_{14}$ is characterised by two different nets M1 and M2 stacked along [001] with intercalated Cl^- ions. The nets consist of $[Sn(OH)_3]^-$ and $[Sn(OH)_2Cl_2]^{2-}$-type group for M1 and $[Sn(OH)_3]^-$ with $[Sn(OH)_2Cl]^-$-type groups for M2 with additionally the cubane group $[Sn_4O_3(OH)]^+$ which is linked by $[Sn(OH)_3]^-$ and $[SnCl]^-$ fragments (see Fig. 5a). All but one of the Sn atoms exhibit the trigonal pyramidal coordination, the distinguished tin has a trigonal bipyramidal one.

Table 1
Summary of ^{119}Sn data for $Sn_{21}Cl_{16}(OH)_{14}O_6$

$\delta_{300\,K}$ (mm s^{-1})[a]	3.22 ± 0.01
$\Delta_{300\,K}$ (mm s^{-1})	1.71 ± 0.02
$d\delta/dT$ (mm s^{-1} K^{-1})	$(-3.4 \pm 0.4)10^{-4}$
$d\Delta/dT$ (mm s^{-1} K^{-1})	$(-3.8 \pm 0.4)10^{-4}$
M_{eff} (amu)	122 ± 14
$d[\ln(A(T)/A(25\,K)]$ (K^{-1})	$(-8.0 \pm 0.5)10^{-3}$
θ_D (K)	151 ± 5
$f_{300\,K}$	0.09 ± 0.02
$f_{77\,K}$	0.51 ± 0.05
$f_{4\,K}$	0.74 ± 0.01

[a] Referred to $BaSnO_3$ at 300 K

Tin valence and bonding type can be determined from the Mössbauer parameters. The isomer shift reflects the electronic density at the probe nucleus, known to depend directly on the valence shell *s* population (n_s) and indirectly on the shielding of *p* population (n_p). Compounds of divalent tin have isomer shift from 2.3 to 4.44 mm s^{-1}, at 77 K and relative to $BaSnO_3$ at room temperature [11]. According to the equation $\delta = 3.01n_s - 0.20n_s^2 - 0.17n_sn_p - 0.38$ of Lees and Flinn [12] for isomer shift at 77 K, where n_s and n_p are the 5*s*- and 5*p*-electron population, an ideal stannous ion ($5s^2$) should have an isomer shift of 4.84 mm s^{-1} (see Fig. 6). When crystal field effects give rise to 5*s*–5*p* hybrid orbitals, the charge density at the nucleus is reduced. The isomer shift is reduced and its value is determined by the occupation of the 5*p* state. For the tin(II) compounds at room temperature, if we assume that the total electron density (n_s+n_p) corresponds to exactly two electrons, we obtain $\delta = 4.77 - 2.58n_p - 0.018n_p^2$. The number of *p* electrons deduced from this relation for an isomer shift of 3.22 mm s^{-1} is 0.60.

Most known tin(II) compounds containing tin atoms in a distorted pyramidal environment have large quadrupole splitting [13]. This splitting $\Delta = 1.71$ mm s^{-1} is induced by the electric field gradient (EFG) and thus by the local environment distortion. In covalently bonded tin compounds, the 5*s* and 5*p* orbital are hybridised and the tin lone pair not used for bonding is located on one of the hybrid orbitals that are highly axial. This lone pair is

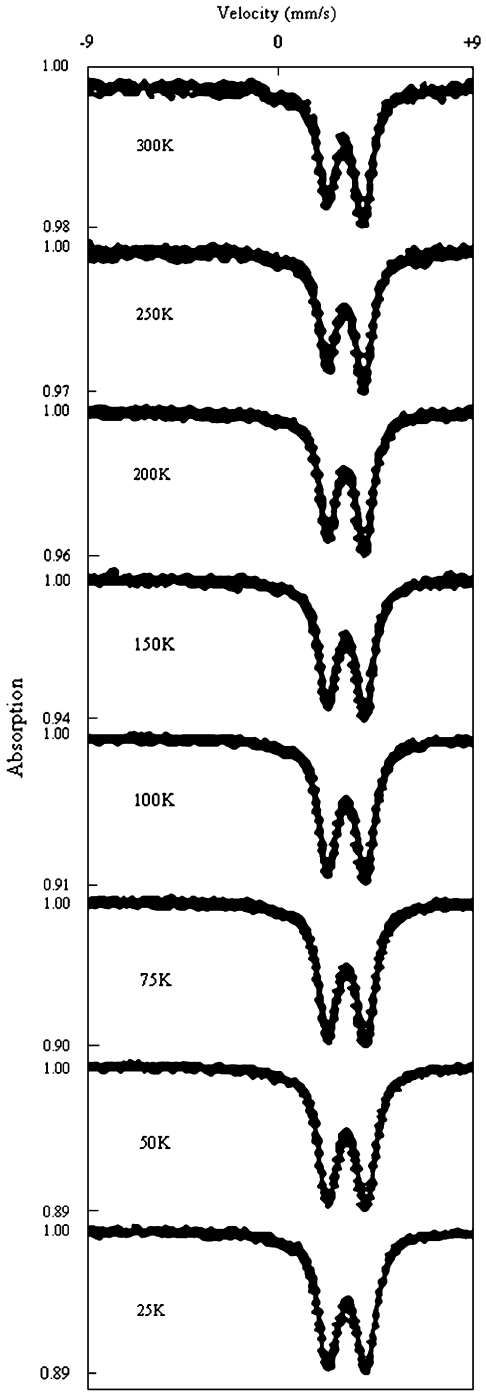

Fig. 4. Mössbauer spectra of $Sn_{21}Cl_{16}(OH)_{14}O_6$ at various temperatures.

stereoactive and distorts the tin polyhedron of coordination. In such ordered structures, bonding requirements make the lone pairs of neighbouring tin atoms cluster in sheets that are highly efficient cleavage plane, resulting in strongly two-dimensional structures, generating well-crystallised platelets as observed in Fig. 1. The lone pair points towards the interlayer space creating a Van Der Waals gap and gives rise to the EFG detectable by ^{119}Sn Mössbauer spectroscopy. This anisotropic electron distribution in the valence shell of the Mössbauer atom is the usually called "valence electron contribution" to the EFG. The distant ions surrounding the Mössbauer atom in non-cubic symmetry is the second source able to contribute to the total EFG, usually termed "lattice contribution". Tin has six types of crystallographic environments in $Sn_{21}O_6Cl_{16}(OH)_{14}$ (Fig. 5b), nevertheless only one doublet is observed in the Mössbauer spectrum. This reflects the predominance of the intrinsic contribution to the EFG, in agreement with calculations by Donaldson et al. [14] for a number of tin compounds, showing that the lattice contribution to the EFG at the tin nucleus can be neglected compared to the intrinsic one. So the various environments of tin in $Sn_{21}O_6Cl_{16}(OH)_{14}$ cannot be underlined therefore only one doublet is detectable contrary to the observations reported by Von Schnering et al.

If crystal field effects are the dominant effects giving rise to the EFG at the tin nucleus, the quadrupole splitting is expected to be proportional to the amount of p character in the ground state (the predicted curve is plotted as the dashed upper line in Fig. 6) [11]. An increase in quadrupole splitting with decrease in 5s character is effectively expected. Our experimental data of hyperfine parameters of synthetic abhurite-type compound are reported in Fig. 6. Both crystal field and covalent bonding effects can significantly explain the chemical shift of $Sn_{21}O_6Cl_{16}(OH)_{14}$.

The thermal evolution of the centre shift δ and Δ are shown in Fig. 7a. The temperature dependence of the centre shift δ results from the variation of two contributions, the δ_{IS} due to chemical shift, and the dominating shift δ_{SOD} due to second-order Doppler effect.

As expected, the temperature dependence of δ for $Sn_{21}O_6Cl_{16}(OH)_{14}$ in the temperature range $25 \leqslant T \leqslant 300$ K is well fitted by a linear relationship. The correlation coefficient to the linear regression is 0.994. From this temperature dependence an effective vibrating mass M_{eff} of the recoiling unit can be calculated using the following relationship [15]:

$$\frac{d\delta}{dT} = -\frac{3}{2}\frac{E_\gamma k_B}{M_{eff}c^2} \quad (1)$$

in which E_γ is the Mössbauer γ-ray energy and k_B the Boltzmann constant. From the slope $d\delta/dT = -3.4 \times 10^{-4}$ mm s^{-1} K^{-1}, a M_{eff} value of 122 amu is determined.

The quadrupole splitting of $Sn_{21}O_6Cl_{16}(OH)_{14}$ over the above temperature range is also slightly temperature dependent, it increases with decreasing temperature (Fig. 7a). The correlation coefficient to the linear regression is 0.992 and the slope $d\Delta/dT = -3.8 \times 10^{-4}$ mm s^{-1} K^{-1} is close to the slope determined from the isomer shift temperature dependence. The temperature dependence of the quadrupole splitting means a fluctuation of the charge distribution around tin nucleus. This T dependence of the quadrupole splitting may result in anisotropy in the thermal expansion of the $Sn_{21}O_6Cl_{16}(OH)_{14}$ lattice in this temperature range.

The asymmetry observed in the quadrupole doublet could associated to the presence of more than one doublet or be caused either by the Goldanskii–Karyagin effect remaining from the vibrational anisotropy in the crystal, or a preferred orientation of the $Sn_{21}O_6Cl_{16}(OH)_{14}$ grains. Indeed, owing to the local electronic environment around the metal atom in such compound it is plausible that there may be vibrational anisotropy in the Sn motion parallel and perpendicular to the symmetry axis, as well as crystal-orientation effects because of the resulting plate-like crystallographic morphology, or several detectable sub-spectra with different sets of parameters. This third assumption, that we previously set aside, will be ruled out in the next section. The Goldanskii–Karyagin effect is temperature dependent while the asymmetry caused by the preferred orientation is not. In order to conclude, the area ratio A_1/A_2 of the two components of the doublet, obtained from a sample carefully grinded in order to favour random orientation of the crystals with respect to the optical axis of the Mössbauer experiment, was plotted versus the temperature as shown in Fig. 7b. The experimental data were well fitted with a straight line (correlation coefficient is 0.982) which

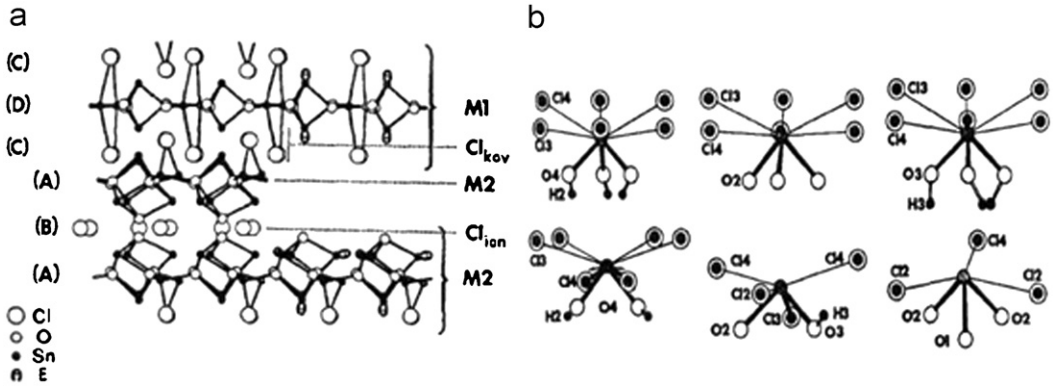

Fig. 5. (a) Crystal structure of $Sn_{21}Cl_{16}(OH)_{14}O_6$ packing along c (the partial structure is projected onto (100)): sequence of the two-dimensional infinite structure-motives M1 and M2 with intercalated Cl^- ions (M2, $[Cl^-]_4$, M2, M1). (b) Representation of the six environments of tin atoms in abhurite. From Ref. [3].

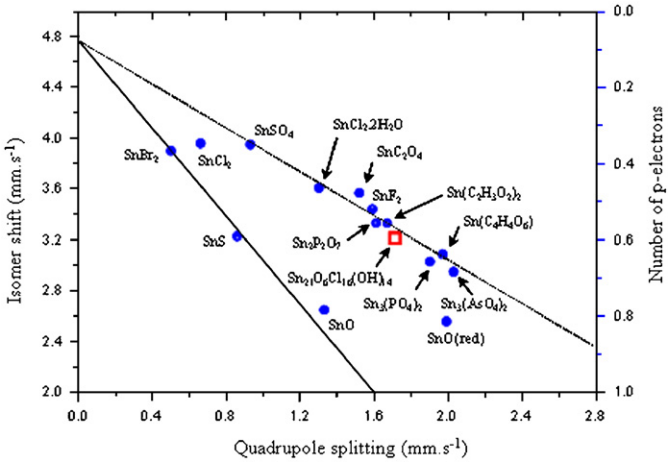

Fig. 6. Relation between isomer shift and quadrupole splitting for stannous compounds from Ref. [12], the dashed and continuous lines represent, respectively, crystal field and spin–orbit effects. $Sn_{21}O_6Cl_{16}(OH)_{14}$ position is represented by the □ symbol.

approaches the ratio $A_1/A_2 = 1$ in the low temperature limit. The difference between the real $T = 0\,K$ intercept and unity is not greater than about 0.02, which is approximately the experimental error assigned to the present data. Consequently, the temperature dependence of the ratio is dominated by temperature-dependent phenomena and cannot be due principally to remaining crystal-orientation effects. So the asymmetry can be essentially attributed to anisotropy of atomic vibrations according to the Goldanskii–Karyagin effect.

4.2. Temperature dependence of the recoil-free fraction

The recoil-free fraction, f, is the fraction of all emission or absorption events in which no vibrational phonon of the lattice is involved. In the approximation of harmonic lattice vibrations the recoil-free fraction is given by

$$f = \exp(-K^2\langle x^2\rangle) \tag{2}$$

in which K is the wave vector of γ radiation and $\langle x^2\rangle$ is the mean square amplitude of vibrations parallel to the γ-rays propagation axis. Since this vibrational amplitude is temperature dependent, the recoil-free fraction itself is temperature dependent. The most frequently used treatment of the temperature dependence of this lattice parameter is the Debye model [16] from which f can be written as

$$f = \exp\left[\frac{-3E_R}{2k_B\theta_D}\left(1 + 4\left(\frac{T}{\theta_D}\right)^2\right)\int_0^{\frac{\theta_D}{T}}\frac{y\,dy}{\exp(-y)-1}\right] \tag{3}$$

in which θ_D is the so-called Mössbauer lattice temperature, and E_R is the recoil energy, ($E_R = 2.572\times10^{-3}$ eV for ^{119}Sn nuclei). With Eq. (3) it appears that the free-recoil fraction can be calculated only if θ_D is determined. In the thin absorber approximation, the temperature dependence of the absorber recoil-free fraction is well represented by the thermal evolution of the absorption area A. In the high temperature limit ($T > \theta_D/2$), Eq. (3) can then be written as

$$\frac{d\ln f}{dT} = \frac{d\ln A}{dT} = -\frac{6E_R}{k_B\theta_D^2} \tag{4}$$

The thermal evolution of the spectrum area (normalised to the area at 25 K) with temperature is shown in Fig. 8a. In the high temperature range, the curve is well fitted by the linear relationship (4). The slope determined, $d\ln[A(T)/A(25\,K)] = -8.0\times10^{-3}\,K^{-1}$, allows to find that $\theta_D = 151$ K. Consequently, using the θ_D value and Eq. (3) the thermal evolution of the recoil-free fraction can be determined as shown in Fig. 8b. This f variation is significant and can have indirect effect on the width of the lines of the spectrum, indeed the absorber thickness is f dependant [17]. Both lines of the spectra become broadened in the same proportion with decreasing T. As slight variations in the EFG or in the electronic configuration of tin atoms are expected to produce a broadening and distortion of the Mössbauer spectrum, structural contribution to the observed broadening will not be considered. For absorber nuclei at infinite dilution in ideal environment, $\Gamma_{absorber} = \Gamma_{natural}$ and the measured full-width at half-maximum $\Gamma = \Gamma_{source}+\Gamma_{natural}$. With line broadening due to absorber thickness it becomes $\Gamma = \Gamma_{source}+\Gamma_{natural}$ $+0.27\Gamma_{natural}n\sigma_0 f_{absorber}$ [18]. The thermal evolution of Γ, expressed through the f variation, is well fitted by a linear relationship (Fig. 9). Extrapolated line width to zero-absorber thickness for this compound gives $\Gamma = 0.864\,mm\,s^{-1}$ (correlation coefficient $R^2 = 0.9976$). This value is in agreement with Γ measured for the $Ba^{119m}SnO_3$ source ($\Gamma_{Ba^{119}SnO_3} = 0.858\pm0.006\,mm\,s^{-1}$). Moreover this result enables to reject one of the three previous assumptions concerning the asymmetry of the spectrum. The adjustment of the spectrum using more than one doublet leads to a line width lower than the width of instrumental line.

The recoil-free fraction of $Sn_{21}O_6Cl_{16}(OH)_{14}$ is determined in this work for the first time. The low value at room temperature $f_{300\,K} = 0.09$ is in the same order than other recoil-free fractions of divalent tin compounds. Usually, in various categories of aggressive

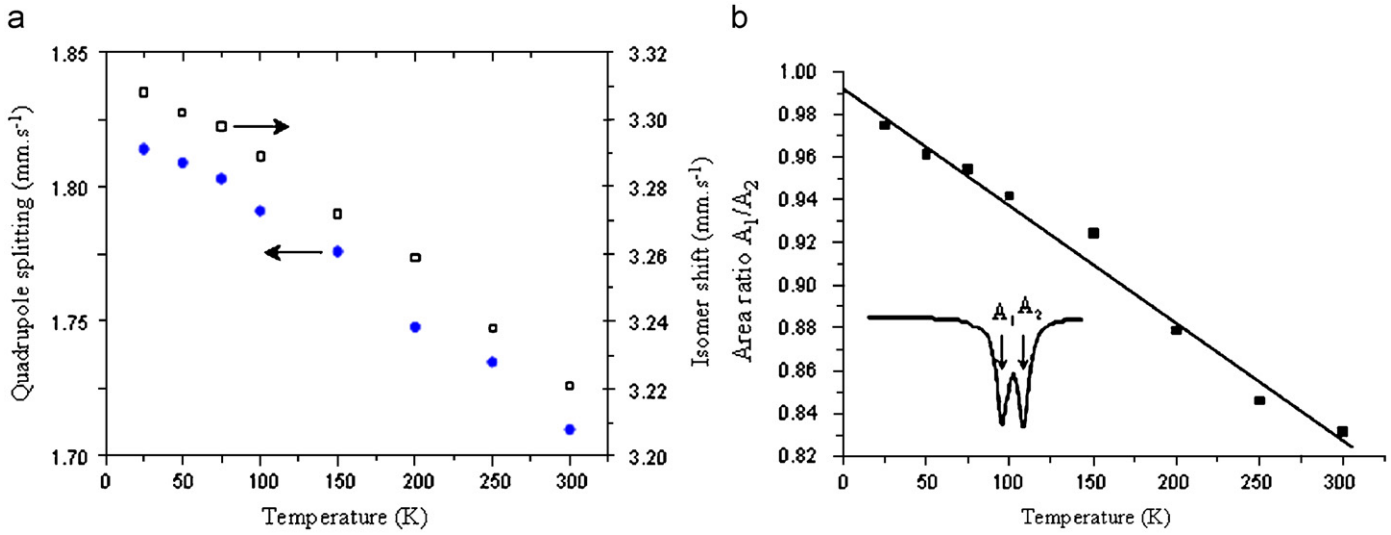

Fig. 7. (a) Temperature dependence of the isomer shift and quadrupole splitting of $Sn_{21}O_6Cl_{16}(OH)_{14}$. (b) Thermal evolution of the area ratio A_1/A_2 of the doublet components of $Sn_{21}O_6Cl_{16}(OH)_{14}$.

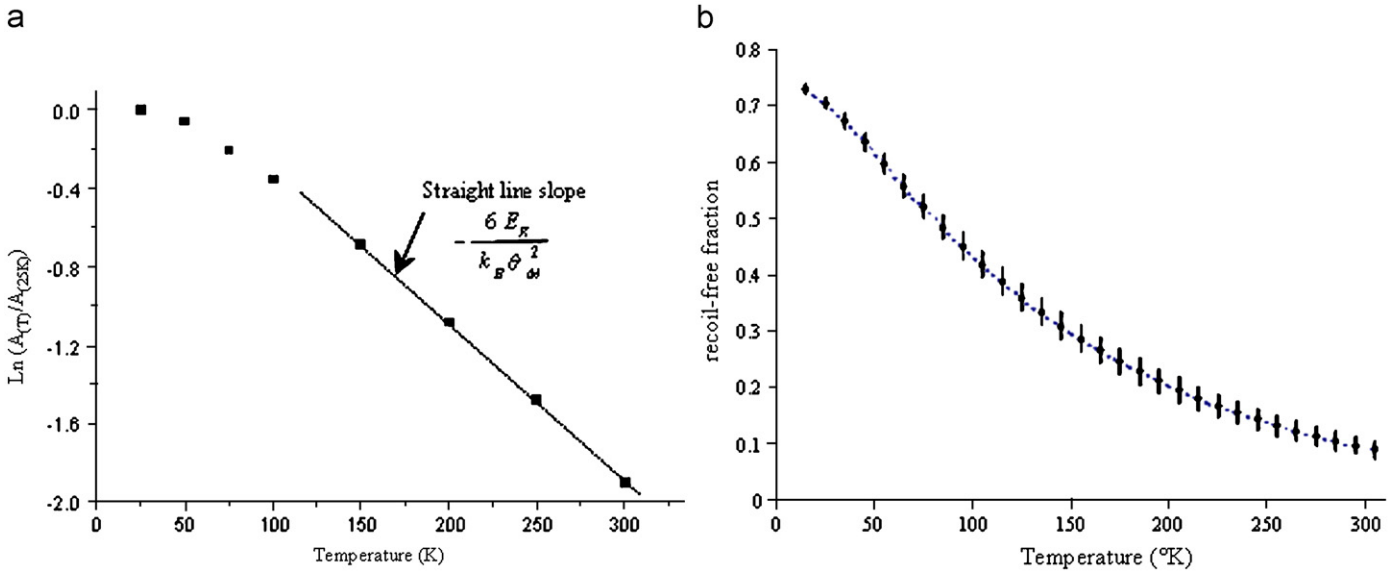

Fig. 8. (a) Temperature dependence of the normalised area under the resonance curve for $Sn_{21}O_6Cl_{16}(OH)_{14}$. (b) Thermal evolution of the recoil-free fraction for $Sn_{21}O_6Cl_{16}(OH)_{14}$.

environments, the corrosion product developed on tin surface is mainly the hydrated stannic oxide $SnO_2 \cdot xH_2O$. At room temperature, this compound has the highest recoil-free fraction ($f_{SnO_2} = 0.46$) among the tin compounds [19]. The large difference between the recoil-free fraction of stannic oxide and tin(II) corrosion products such $Sn_{21}O_6Cl_{16}(OH)_{14}$ is a real problem in room temperature Mössbauer spectroscopy since the area of the sub-spectrum—and thus its detection limit—are directly dependent on this difference. In the light of our results, the weight % detection limit, of the $Sn_{21}O_6Cl_{16}(OH)_{14}$ mixed with stannic oxide, is divided by 4 from room temperature to 4 K. The interest of the low temperature for qualitative measurements is then clearly evident.

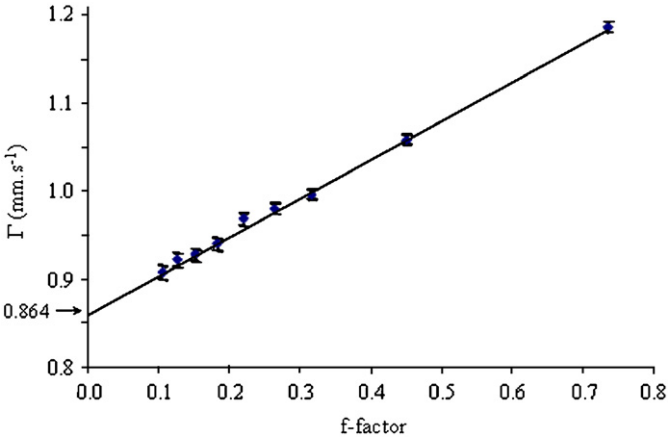

Fig. 9. Temperature dependence of the full-width at half-maximum versus the recoil-free fraction f, for $Sn_{21}O_6Cl_{16}(OH)_{14}$.

5. Conclusion

Synthetic abhurite-type compound $Sn_{21}O_6Cl_{16}(OH)_{14}$ was investigated for the first time by Mössbauer spectroscopy in the

range 25–300K. At room temperature the spectrum of this oxyhydroxychloride is an asymmetric doublet for which the parameters are $\delta = 3.22\,\mathrm{mm\,s^{-1}}$ and $\Delta = 1.71\,\mathrm{mm\,s^{-1}}$. This chemical shift could be explained by both crystal field and covalent bonding effects. The unique doublet detected in spite of the six crystallographic environments of tin nuclei in $Sn_{21}O_6Cl_{16}(OH)_{14}$ reflects that the lattice contribution to the EFG is negligible compared to the intrinsic one. Thermal evolution of the spectrum indicates that the asymmetry originates mainly from a Goldanskii–Karyagin effect. The temperature dependence of the recoil-free fraction $f(T)$ was also determined. Our determination at room temperature gives $f_{300\,K} = 0.09 \pm 0.02$.

References

[1] J.J. Matzko, H.T. Evans, M.E. Mrose, P. Aruscavage, Can. Mineral. 23 (1985) 233–240.
[2] S.E. Dunkle, J.R. Craig, J.D. Rimstidt, Can. Mineral. 41 (2003) 659–669.
[3] H.G. Von Schnering, R. Nesper, H. Pelshenke, Z. Naturforsch. 366 (1981) 1551–1560.
[4] R. Edwards, R.D. Gillard, P.A. Williams, Mineral. Mag. 56 (1992) 221–226.
[5] S. Jouen, B. Lefez, M.T. Sougrati, B. Hannoyer, Mater. Chem. Phys. 105 (2007) 189–193.
[6] S. Jouen, Thesis, University of Rouen, 2000.
[7] S. Jouen, B. Hannoyer, O. Piana, Surf. Interface Anal. 34 (2002) 192–196.
[8] M. Shibuya, K. Endo, H. Sano, Bull. Chem. Soc. Japan 51 (1978) 1363–1367.
[9] M.T. Sougrati, S. Jouen, B. Hannoyer, in: Application of Mössbauer spectroscopy to the study of tin atmospheric corrosion, Eurocorr 2004, Nice, France, 2004.
[10] RRUFF, Database Raman Abhurite, 〈http://rruff.info/〉.
[11] P.A. Flinn, in: G.K. Shenoy, F.E. Wagne (Eds.), Mössbauer Isomer Shift, Amsterdam, 1978, p. 593.
[12] J.K. Lees, P.A. Flinn, J. Chem. Phys. 48 (1968) 882–889.
[13] N.N. Greenwood, T.C. Gibb, Chapman & Hall (Eds.), Mössbauer Spectroscopy, London, 1971.
[14] J.D. Donaldson, D.C. Puxley, M.J. Tricker, Inorg. Nucl. Chem. Lett. 8 (1972) 845.
[15] R.H. Herber, Plenum Press (Ed.), Chemical Mössbauer Spectroscopy, Springer, New York, 1984, pp. 133–355.
[16] W.A. Steyert, R.D. Taylor, Phys. Rev. 134 (1964) A716–A722.
[17] S. Margulies, J.R. Ehrman, Nucl. Instrum. Methods 12 (1961) 131–137.
[18] D.A. O'Connor, Nucl. Instrum Methods 21 (1963) 318–322.
[19] M.T. Sougrati, S. Jouen, B. Hannoyer, Hyperfine Interact. 167 (2006) 815–818.